ChemEurJ

Research Article
doi.org/10.1002/chem.202502837

Chemistry Europe
European Chemical Societies Publishing

www.chemeurj.org

Trigonal Bipyramidal Clusters $[Tl_5]^{7-}$: Synthesis and Characterization of the *Zintl* Phase $K_{7-x}A_xTl_5$ (A = Rb, Cs; $0 < x \leq 2.35$)

Vanessa F. Schwinghammer,[a, b] Tomáš Kovářík,[c] Ilya G. Shenderovich,[a] Ján Minár,[c] and Stefanie Gärtner*[a, b]

In alkali metal thallides, a huge variety of thallium clusters can be realized, which are surrounded only by alkali metals. In most cases, different cluster types are present in the crystal structures at the same time. One example is the $[Tl_5]^{7-}$ trigonal bipyramid, which has only been observed beside $[Tl_9]^{9-}$, $[Tl_4]^{8-}$, $[Tl_3]^{7-}$, $[Tl]^{5-}$, or $[Tl_8Cd_3]^{10-}$. In the new ternary alkali metal thallide phase $K_{7-x}A_xTl_5$ (A = Rb, Cs; $0 < x \leq 2.35$), exclusively $[Tl_5]^{7-}$ clusters are present, and the compound can be described as a salt-like Zintl-phase, where the electron count is balanced in terms of the anionic moiety and counter cations. This phase crystallizes in the orthorhombic noncentrosymmetric space group *Ama*2. Different temperature programs applied during synthesis suggested metastability, which was subsequently proven by DSC measurements. DFT calculations reveal a minimum in the DOS at E_F and support the salt-like description. Dissolution experiments in the style of well-known group 14 and group 15 solution chemistry in liquid ammonia were performed and showed oxidation of the alkali metal thallide. Initial ^{205}Tl NMR studies in liquid ammonia allow for the detection of the first signal of a dissolved thallium species emerging from a thallide Zintl phase.

1. Introduction

Trigonal bipyramidal entities represent an important structural feature known from the chemistry of distinct molecular compounds as well as from solid-state materials. Concerning isolated, homoatomic main group element clusters of group 14, their expected charge can be calculated by applying Wade–Mingos rules,[1,2] as a 5-atom *closo* cluster affords a total number of $(4n + 2) = 22$ electrons ($n = 5$), equivalent to $(n + 1)$ skeletal electron pairs.[3] This in turn yields a twofold negative charge for the expected polyanion $[Tt_5]^{2-}$ (Tt = Si—Pb) ($(5 \times 4\ e^-) + 2e^-$). One can think of realizing this electron count by applying the Zintl–Klemm–Busmann concept[4–10], which is well-known in the world of intermetallic solid-state compounds. There, the less electronegative metal donates its valence electrons to the more electronegative partner, and a polyanionic salt is obtained.[11,12] This, for example, works well for P_4 isoelectronic, tetrahedral $[Tt_4]^{4-}$ anions, which are present in A_4Tt_4 Zintl phases (A = Na—Cs, Tt = Si—Pb).[13–16] In contrast, a hypothetical, simple A_2Tt_5 Zintl phase is not known yet. To produce these trigonal bipyramidal anions, one has to use a solvent route[17,18] by dissolving a higher reduced Zintl phase A_4Tt_4 or $A_{12}Tt_{17}$[19,20] in solvents like liquid ammonia, ethylene diamine, or tetrahydrofuran (THF). The highly reduced $[Tt_4]^{4-}$ cluster units are then oxidized by the solvent to form $[Tt_5]^{2-}$.[21] The use of [2.2.2]-cryptand molecules as a sequestering agent for the alkali metal cations facilitates crystallization of a densely packed crystalline material with the composition of $[Tt_5]^{2-}$: [A@cryptand] of 1:2.[22–27] The crystal structures of the latter are related to the $CaIn_2$ structure type.[22] For isoelectronic five-atom clusters of group 15 elements, the expected charge has to be reduced by five, and this, therefore, is equivalent to a cationic cluster unit. Indeed, $[Bi_5]^{3+}$ cations are reported by the use of an ionic liquid.[28,29] In analogy, one would expect a fivefold higher negative charge for homoatomic five-atom clusters of group 13 elements. These $[Tr_5]^{7-}$ clusters (Tr = group 13 element) have also been reported in alkali metal thallide structures.[30–32] Again, a straightforward binary A_7Tr_5 Zintl phase of the desired alkali metal proportion of 7/12 = 0.583 has not yet been reported. In the binary systems, only one compound $K_{10}Tl_7$ (10/17 = 0.588) is known, but this compound includes the larger $[Tl_7]^{7-}$ clusters.[33] Additional three electrons are responsible for the metallic character of the latter compound. The absence of a hypothetical A_2Tt_5 Zintl phase is somehow comprehensible, as an efficient packing of the salt might be prevented by the unfavorable ratio of large $[Tt_5]^{2-}$ clusters and only two counter cations. In contrast, the availability of sufficient alkali metal atoms to allow a dense packing makes the absence of electron precise A_7Tr_5 according to Wade's

[a] V. F. Schwinghammer, I. G. Shenderovich, S. Gärtner
Central Analytics, University of Regensburg 93040, Regensburg, Germany
E-mail: Stefanie.Gaertner@ur.de

[b] V. F. Schwinghammer, S. Gärtner
Department of Inorganic Chemistry, University of Regensburg 93040, Regensburg, Germany

[c] T. Kovářík, J. Minár
New Technologies Research Center Pilsen, University of West Bohemia in Pilsen, Pilsen 301000, Czech Republic

Supporting information for this article is available on the WWW under https://doi.org/10.1002/chem.202502837

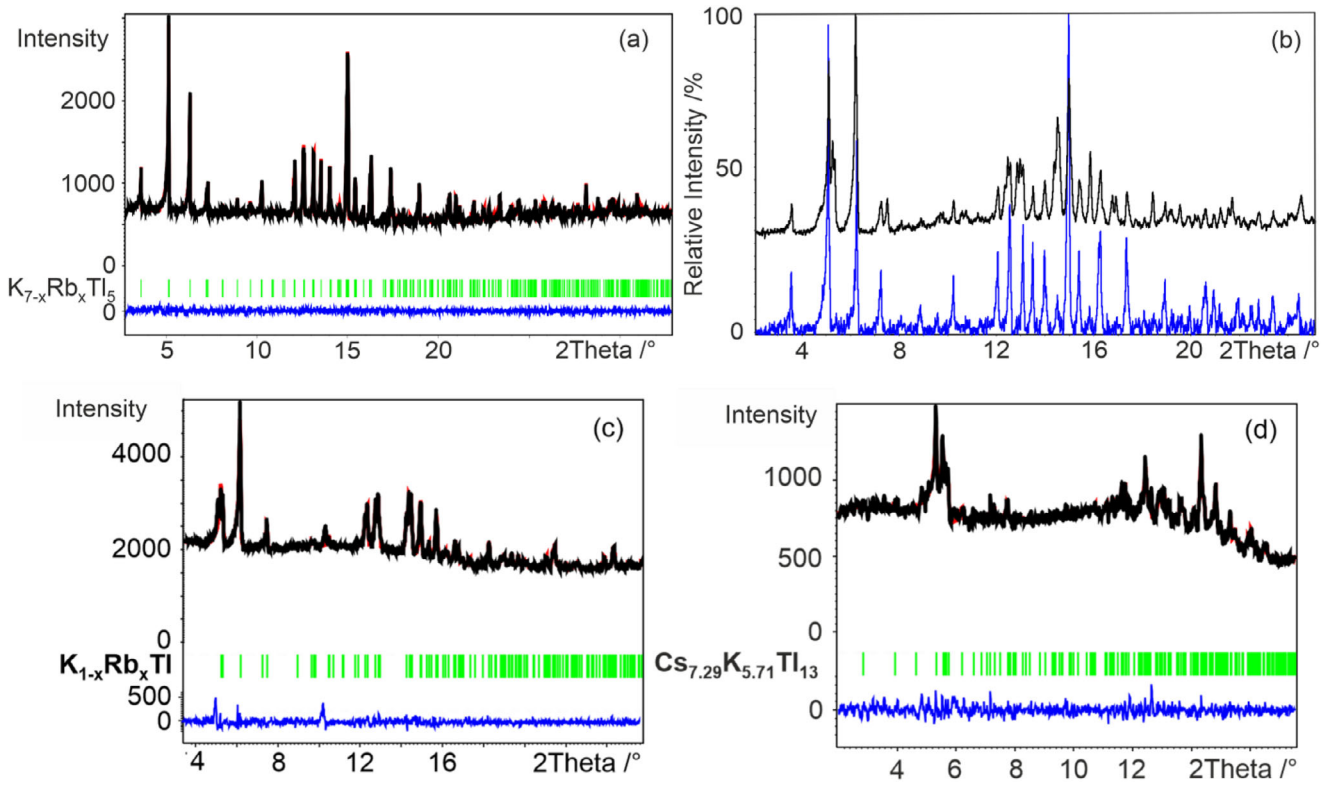

Figure 1. Measured powder diffraction patterns of the samples with the nominal compositions $K_8Rb_2Tl_7$ a), K_6RbTl_5 (b: temperature program 2 (quenching and annealing):black; temperature program 3 (quenching): blue), $K_4Rb_3Tl_5$ c), and $K_4Cs_3Tl_5$ d). The refinement was carried out with the LeBail algorithm (a, c, d) in Jana2006. The calculated reflection positions are shown by the vertical bars (green) underneath the powder pattern, and the calculated intensities as a red curve. The curve at the bottom (blue) represents the difference plot. (a) GOF = 0.77, R_p = 2.10, R_{wp} = 2.73; (c) GOF = 0.99, R_p = 1.58, R_{wp} = 2.17; (d) GOF = 0.87, R_p = 2.51, R_{wp} = 3.31. x-axis: 2Theta in °, y-axis: intensity.

rules less intuitive. In general, trigonal bipyramidal units are a very frequent structural motif in intermetallic compounds, as topologically close-packed phases are dependent on tetrahedra being present, and the trigonal bipyramidal unit is the central assembly unit in double tetrahedral stars. These double tetrahedral stars are also known for alkali metal trielides.[34] In the A_8Tr_{11} structure, these entities are present[35–39] and due to very similar Tl-Tl and Na-Tl distances,[40,41] a similar arrangement according to "Na_6Tl_5" for a Tl_5 cluster is observed in the above-mentioned mixed alkali metal compounds.[30–32] We recently showed that mixed alkali metal approaches, including the heavier alkali metals, allow the formation of several new electron-precise phases of the trielides.[42–45] These salt-like materials offer investigations in terms of solution chemistry, which is well-known for the higher group Zintl phases, but is missing for trielides. In general, the first step is the preparation of a salt-like material including isolated cluster units. Subsequently, dissolution studies can be carried out.

In the following, the successful mixed alkali metal approach for preparing the first electron-precise, metastable A_7Tl_5 Zintl phase is reported on. Temperature program adjustments, DSC measurements, and DFT calculations of the new ternary alkali metal thallide phase $K_{7-x}A_xTl_5$ (A = Rb, Cs; $0 < x \leq 2.35$) containing $[Tl_5]^{7-}$ trigonal bipyramids as the exclusive thallium unit are presented. Liquid ammonia is known to be the best solvent for the congruent dissolution of highly reduced Zintl phases.[12,21] Therefore, subsequent experiments, including first ^{205}Tl NMR spectroscopic investigations, have been performed to elucidate the reactivity of the new Zintl phase according to the well-established group 14 and group 15 Zintl anion chemistry. In this context, the first ^{205}Tl NMR signal derived by dissolution of a thallide in liquid ammonia could be detected.

2. Results and Discussion

2.1. Synthesis and Crystal Structure Determination

The first approaches to this class of material were prepared in a 10:7 atomic ratio of alkali metal to thallium. The original purpose was to substitute rubidium or cesium in the $K_{10}Tl_7$ structure type.[33] Instead, the powder diffraction pattern and screening of single crystals of the sample with the nominal composition $Rb_2K_8Tl_7$ showed reflections of a new phase with the alkali metal to thallium atomic ratio 7:5. For this reason, the elements in this specific ratio $K_{7-x}A_xTl_5$ (A = Rb, Cs; x = 0–7) were prepared in tantalum ampoules and heated in the furnace at different temperature programs.

The binary samples with the nominal composition A_7Tl_5 (A = K, Rb, or Cs) showed a mixture of KTl[46] and $K_{10}Tl_7$,[33] and in the case of rubidium and cesium, a sticky habitus with single

Table 1. Crystallographic data of $K_{7-x}A_xTl_5$ (A = Rb, Cs; $0 < x \leq 2.35$) from single crystals.

Composition	$K_{6.33}Rb_{0.67}Tl_5$	$K_{4.65}Rb_{2.35}Tl_5$	$K_{6.03}Cs_{0.97}Tl_5$	$K_{5.58}Cs_{1.43}Tl_5$
CSD number	2 464 820	2 464 825	2 464 819	2 464 818
Molar mass /(g/mol)	1326.50	1404.52	1386.78	1429.23
Temperature /K	123			
Crystal system	Orthorhombic			
Space group	*Ama*2			
Cell parameter /Å	$a = 11.0222(6)$	$a = 11.1147(6)$	$a = 11.1459(6)$	$a = 11.2018(7)$
	$b = 22.3132(12)$	$b = 22.5275(14)$	$b = 22.3628(11)$	$b = 22.5084(15)$
	$c = 8.3757(4)$	$c = 8.4248(5)$	$c = 8.3677(4)$	$c = 8.3550(6)$
Volume /Å^3	2059.92(19)	2109.5(2)	2085.68(18)	2106.6(2)
Z	4			
ρ_{calc} /(g/cm^3)	4.277	4.422	4.416	4.506
μ /(mm^{-1})	22.559	44.337	22.291	22.428
F(000)	2200.0	2321.0	2292.0	2357.0
Crystal size /mm^3	0.09 × 0.044 × 0.04	0.053 × 0.03 × 0.026	0.092 × 0.073 × 0.064	0.08 × 0.061 × 0.047
Radiation, λ /Å	Ag Kα, 0.56087	Mo Kα, 0.71073	Ag Kα, 0.56087	Ag Kα, 0.56087
2θ range /°	5.032–61.312	5.148–60.984	5.014–55.726	5.008–55.728
Index ranges	$-20 \leq h \leq 19$	$-15 \leq h \leq 15$	$-18 \leq h \leq 15$	$-18 \leq h \leq 17$
	$-40 \leq k \leq 40$	$-31 \leq k \leq 32$	$-37 \leq k \leq 37$	$-31 \leq k \leq 37$
	$-14 \leq l \leq 15$	$-12 \leq l \leq 11$	$-13 \leq l \leq 13$	$-13 \leq l \leq 12$
Reflections collected/independent	19 331/6530	22 459/3335	16 647/4829	11 360/4836
data/restraints/parameter	6530/1/65	3335/1/67	4829/1/65	4836/1/65
GooF	1.005	1.022	1.061	1.045
R_{int}	0.0507	0.0641	0.0386	0.0351
R_1, wR_2 [I > 2σ(I)]	0.0378, 0.0581	0.0275, 0.0618	0.0277, 0.0654	0.0507, 0.1060
R_1, wR_2 [all data]	0.0490, 0.0622	0.0330, 0.0634	0.0301, 0.0671	0.0582, 0.1097
$\Delta\rho_{max,min}$ /eÅ^{-3}	3.54/−2.51	1.97/−0.87	2.19/−1.54	2.49/−2.38
Flack	−0.029(13)	0.103(10)	−0.010(11)	−0.02(2)

crystals of Rb_8Tl_{11}[36,39] or CsTl.[47] Ternary approaches revealed that both potassium and a small proportion of rubidium or cesium are necessary for the formation of this phase. It was noticed that an increased proportion of rubidium or cesium relative to potassium results in a more ductile product. Figure 1 shows the powder diffractograms of the nominal preparations $K_8Rb_2Tl_7$ (a) and K_6RbTl_5 (b), whereby in the latter preparation, two different temperature programs, TP2 (black) and TP3 (blue), were compared with each other. The biggest difference between them is that in the diffractogram shown in black, in addition to the $K_{7-x}Rb_xTl_5$ reflections, KTl can also be identified, which could have been caused by the tempering following the quenching during the synthesis. According to the powder diffractogram, the approaches with the nominal composition $K_4A_3Tl_5$ (*A* = Rb, Cs) no longer contain the desired phase. In the case of rubidium, $K_{1-x}Rb_xTl$ is formed in addition to a soft mass, whereas in the nominal approach, $K_4Cs_3Tl_5$, the compound $Cs_{7.29}K_{5.71}Tl_{13}$ is formed together with a soft mass.[42,43]

Several crystals from the various samples were analyzed using single crystal X-ray diffraction (SCXRD) for $K_{6.33}Rb_{0.67}Tl_5$, $K_{4.65}Rb_{2.35}Tl_5$, $K_{6.03}Cs_{0.97}Tl_5$, and $K_{5.58}Cs_{1.42}Tl_5$. The phase with variable rubidium or cesium content crystallizes in the orthorhombic space group *Ama*2. The crystallographic data are given in Table 1 (for SEM/EDS see Supporting Information).

2.2. Structure Description

In the $K_{7-x}A_xTl_5$ phase (*A* = Rb, Cs; $0 < x \leq 2.35$), $[Tl_5]^{7-}$ trigonal bipyramids are present as anionic moieties (see Figure 2). This is built up by four crystallographically different thallium positions Tl1-Tl4 (Tl1: Wyckoff 8*c*, Tl2-Tl4: Wyckoff 4*b*).

The clusters are arranged in hexagonal layers with the stacking sequence ABAB, which results in a distorted hexagonal close packed structure (see Figure 3). The trigonal bipyramids are separated from each other by alkali metal atoms, which consist of five crystallographically different positions. The first coordination sphere of the thallium units contains 19 alkali metal atoms ($d(A\_Tl) < 4.1$ Å). All triangular faces except those spanned by Tl1, Tl1#, and Tl2 or Tl4 are μ^3 capped by one alkali metal each. The equatorial-axial and Tl1-Tl1# edges are each μ^2 coordinated by one atom. In addition, at least one alkali metal atom is present at each cluster corner, with two alkali metals at Tl2–Tl4.

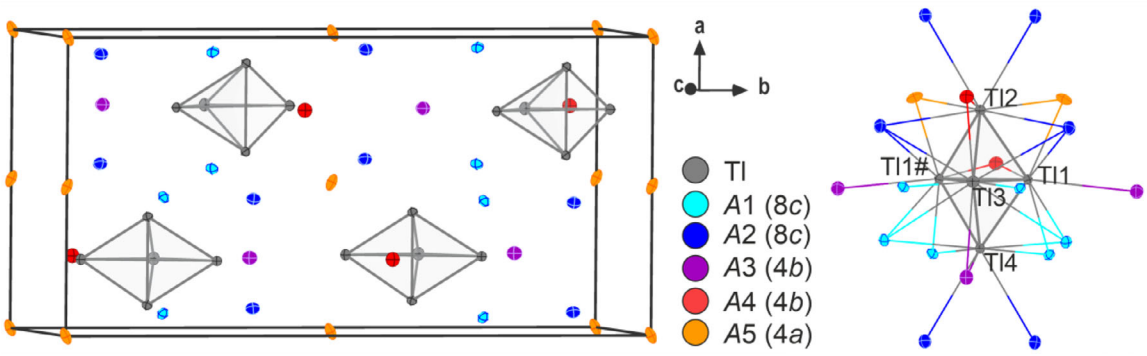

Figure 2. Unit cell of the phase $K_{7-x}A_xTl_5$ and the first coordination sphere of the $[Tl_5]$ trigonal bipyramid. The atom marked with # is generate with (1/2_x, y, z).

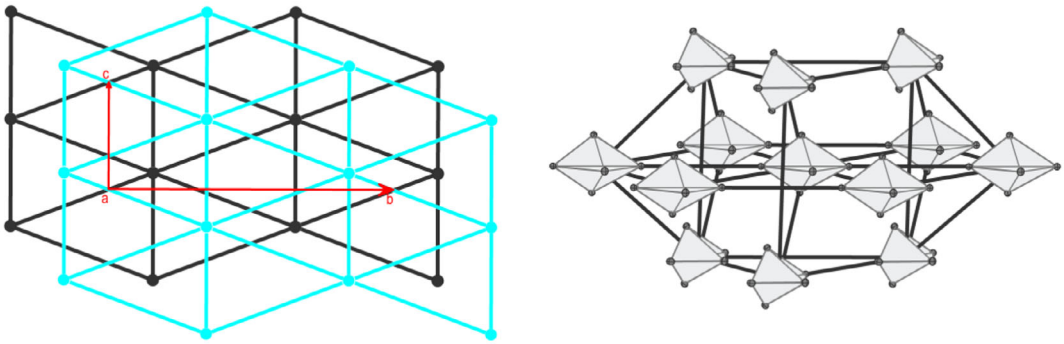

Figure 3. Hexagonal layers of the $[Tl_5]^{7-}$ trigonal bipyramids perpendicular to the crystallographic a-axis and the cluster arrangements.

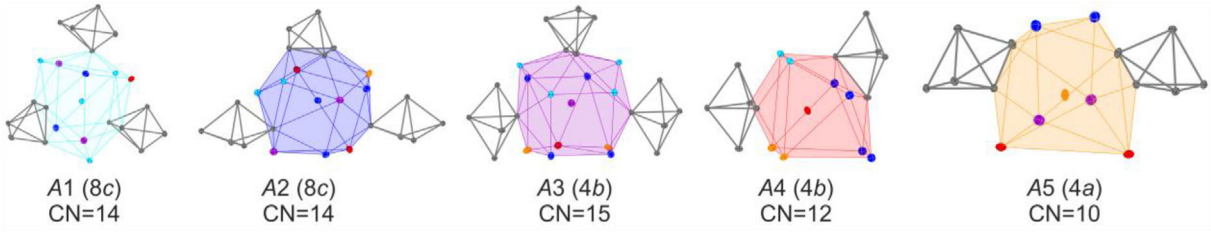

Figure 4. The first coordination sphere of the five crystallographically different alkali metal positions in $K_{7-x}A_xTl_5$.

The alkali metals are divided into five crystallographically different positions. The coordination numbers of the first coordination sphere of these alkali metal positions vary between 10, 12, 14, and 15 (see Figure 4). The environments can be distinguished into coordination with three (*A*1–*A*3) and two (*A*4, *A*5) trigonal bipyramids. At least two of the alkali metal positions are mixed with potassium and rubidium or cesium, whereby in the composition $K_{4.65}Rb_{2.35}Tl_5$, four positions are mixed (*A*1–*A*4). The highest rubidium or cesium content is found at alkali metal position *A*3 (Wyckoff 4*b*) (see Table 2). This is consistent with the earlier observations about the relationship between coordination number and occupancy factor.[42,43] This results in the order *A*3 (Wyckoff 4*b*) > *A*2 (Wyckoff 8*c*) > *A*4 (Wyckoff 4*b*) > *A*1 (Wyckoff 8*c*) > *A*5 (Wyckoff 4*a*) for the positions with the highest rubidium or cesium content to the lowest. The slight discrepancy in the order of *A*1 and *A*4 can probably be explained by the slightly different volumes of the coordination polyhedra (V(*A*1) = 21.3432 Å^3, V(*A*4) = 23.3766 Å^3).

2.3. Temperature-Dependent Measurements

For DSC measurements, the sample with the nominal composition $Rb_2K_8Tl_7$ was examined. The applied cooling protocol at a rate of 1 K/min corresponds to a slow cooling regime, enabling verification of the metastability of the phase $K_{7-x}A_xTl_5$. The DSC trace exhibits three distinct thermal events: two endothermic transitions upon heating and one exothermic transition during cooling (see Figure 5).

The first endothermic peak (No.1) observed during the heating cycle (onset: 389.71 K) is attributed to a solid-solid transformation. The second endothermic event (onset: 490.40 K) suggests congruent melting of the primary solid-state phase (Figure 5, No.2), especially since above 521.60 K, no significant thermal effect is visible. Upon subsequent cooling, a single exothermic peak (No.3, onset: 531.30 K) is detected, indicating recrystallization of the melt into the main phase corresponding to peak No.2.

Table 2. Site occupancy factors (s.o.f) of the five crystallographically different alkali metal positions in $K_{7-x}A_xTl_5$ (A = Rb, Cs; 0 < x < 2.35).

Composition	s.o.f.(*A*1)		s.o.f.(*A*2)		s.o.f.(*A*3)		s.o.f.(*A*4)		s.o.f.(*A*5)	
$K_{6.33}Rb_{0.67}Tl_5$	K	1	K	0.866(6)	K	0.608(10)	K	1	K	1
	Rb	0	Rb	0.134(6)	Rb	0.392(10)	Rb	0	Rb	0
$K_{4.65}Rb_{2.35}Tl_5$	K	0.914(11)	K	0.455(11)	K	0.124(18)	K	0.785(19)	K	1
	Rb	0.086(11)	Rb	0.545(11)	Rb	0.876(18)	Rb	0.215(19)	Rb	0
$K_{6.03}Cs_{0.97}Tl_5$	K	1	K	0.883(5)	K	0.261(7)	K	1	K	1
	Cs	0	Cs	0.117(5)	Cs	0.739(7)	Cs	0	Cs	0
$K_{5.58}Cs_{1.43}Tl_5$	K	1	K	0.724(8)	K	0.129(13)	K	1	K	1
	Cs	0	Cs	0.276(8)	Cs	0.871(13)	Cs	0	Cs	0

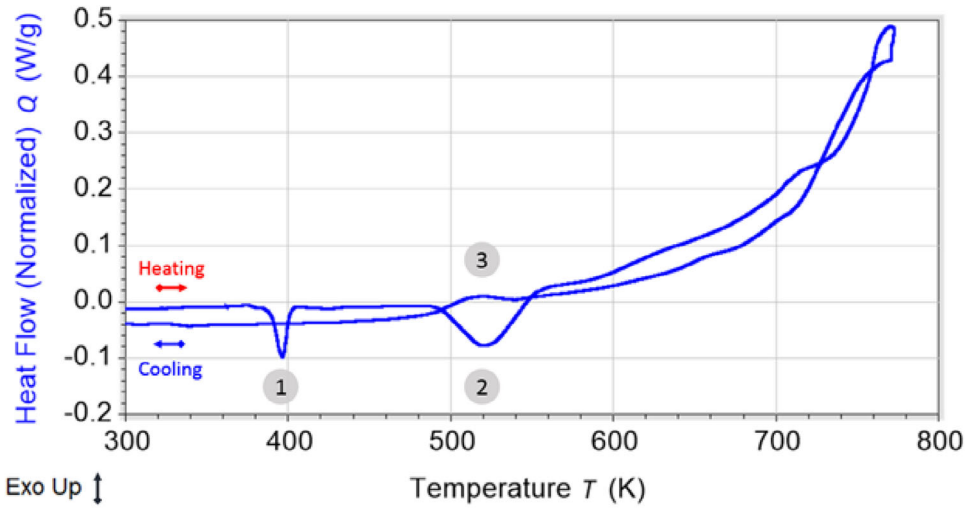

Figure 5. DSC curve of the sample with the nominal composition $Rb_2K_8Tl_7$ (Tzero hermetic aluminium pan, purge flow: N_2 40 mL/min).

A summary of the peak effects of the thermal events is provided in the Supporting Information.

Additional temperature-dependent PXRD studies (see Supporting Information) showed an irreversible phase change from $K_{7-x}Rb_xTl_5$ to $K_{1-x}Rb_xTl$.[42,46] These results corroborate earlier indications of the metastability of the phase $K_{7-x}A_xTl_5$ (*A* = Rb, Cs) obtained during the synthesis with different temperature programs and the DSC results.

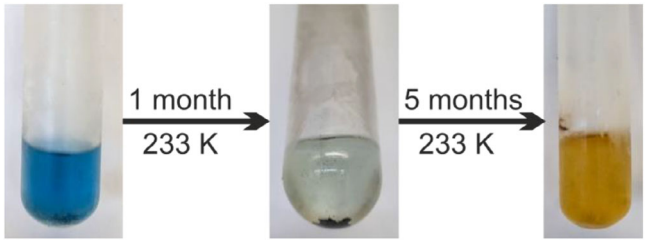

Figure 6. Observations of the solubility tests in liquid ammonia. First blue color after condensation, second after one months of storage at 233 K, and last orange color and red solid at the glass vessel after additional five months of storage at 233 K.

2.4. Dissolution Experiments in Liquid Ammonia

Liquid ammonia is well-suited for congruently dissolving highly negatively charged homoatomic polyanions. Previous studies on the solubility of alkali metal thallides in liquid ammonia showed an oxidation to elemental thallium and the formation of alkali metal amide.[45]

Here, in all solubility tests, a dark blue colour of the solution has been observed (Figure 6), which indicates solvated electrons.[48] After approximately one month of storage at 233 K, the liquid became colourless with sediment (Figure 6). The solubility test with the approach with nominal composition K_6CsTl_5 was evaporated after two months of storage, and the residue was analysed using PXRD. The reflection profile of elemental thallium is clearly visible in the powder diffraction pattern (see Supporting Information, Figure S1). It has to be noted that PXRD is not capable of detecting a potential amorphous material.

After another four to five months of storage, orange-brown streaks emanating from the residue and the first brown solid on the vessel wall could be observed (Figure 6). Initial X-ray diffraction experiments on the orange-brown solid from the glass wall showed no reflections. Despite a very long crystallization time, continuous crystallization studies are in progress.

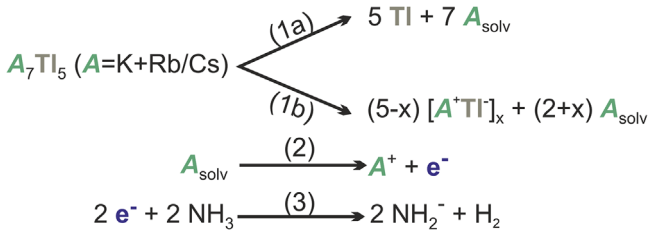

Figure 7. Alkali metal thallide $K_{7-x}A_xTl_5$ possibly is either oxidized to form elemental Tl0 (1a) or a less reduced thallide species (1b). In both cases, the remaining alkali metal (2) formally reduces H^+ from ammonia, yielding (3) amide NH_2^- and elemental hydrogen H_2.

2.5. NMR Studies

For a better understanding of the dissolution behavior of alkali metal thallides in liquid ammonia, ^{1}H and ^{205}Tl NMR measurements were carried out. Due to the sensitivity of the compound, the sample was prepared in analogy to the well-established NMR investigations on alkali metal silicides.[49–51] In addition to the dominant NH_3 resonance, the ^{1}H NMR spectra recorded between 203 and 233 K display two singlets (see Figure 8, left), assignable to the amide NH_2^- anion (−2.44 ppm) and to dissolved elemental hydrogen (4.57 ppm). This is in accordance with the oxidation of $K_{7-x}A_xTl_5$ to elemental thallium (Figure 7, (1a)), which was also observed in the powder diffraction pattern of the residue (see Supporting Information, Figure S1). Dissolved alkali metal A_{solv} yields solvated electrons in liquid ammonia solution (Figure 7, (2)), which form elemental hydrogen and amide with ammonia (Figure 7, (3)). In general, the observation of both the products hydrogen and amide in a fresh sample can mean both: formation of an oxidized thallium species in solution and/or formation of elemental thallium in solid-state (Figure 7). The ^{205}Tl NMR spectra of the solution exhibit, in the temperature range 203–233 K, a broad signal whose chemical shift changes reversibly from about −960 ppm at 203 K, to −1230 ppm at 218 K, and to −1480 ppm at 233 K (see Figure 8, right). This severe temperature dependence is also known for $TlNO_3$ in liquid ammonia, where the Tl^+ assigned signal is shifted from +1790 to +1935 ppm.[52] For $TlNO_3$, also strong effects of the concentration of the salt are observed. At higher temperatures, neither the minor singlets in the ^{1}H NMR spectra nor the signal in the ^{205}Tl NMR spectra are detectable, presumably due to exchange processes. No changes in these spectra were observed after two months of storage at 233 K. In order to gain further insights concerning the assignment of the signal, additional NMR experiments are needed, which address Tl^+ in liquid ammonia solution, in dependence on different counter anions, especially weakly coordinating anions.

2.6. DFT Calculations

The compositions A_7Tl_5 (A = K, Rb), K_6ATl_5 (A = Rb, Cs), and $K_4Rb_3Tl_5$ without mixed-occupied positions were used to calculate the electronic structures. The aim here was to find out to what extent the heavier homologues rubidium and cesium influence the electronic situation. The program FPLO21[53–56] was used for the calculation. The DOS plots of the various compositions in the range from −2 to 2 eV show only minimal differences and all exhibit a pseudo band gap at the Fermi level (see Figure 9).

A closer look at the band structure and DOS using the example K_6RbTl_5 reveals localized states in the range from −9 to −4 eV, which are predominantly assigned to the thallium 6 s states (see Figure 10). These can be divided into the apical (Tl2, Tl4: approx. −6 and −4 eV) and equatorial thallium positions (Tl1, Tl3: −5.5 to −5 eV) of the $[Tl_5]^{7-}$ cluster. This is a common characteristic of substances made up of components with little interplay.[57] The thallium 6p and alkali metal states dominate around the Fermi level.

DFT calculations showed an area with localized bands, which can be assigned to the different thallium atoms, and an area with large dispersion around the Fermi level. Due to the pseudo band gap, the material is a classical semi metal.

3. Conclusion

We here report on the synthesis and characterization of the ternary phase $K_{7-x}A_xTl_5$ (A = Rb, Cs; $0 < x \leq 2.35$). Single crystal X-ray analysis reveals the presence of $[Tl_5]^{7-}$ trigonal bipyramids as the exclusive cluster type. This is special, because until now this cluster type was only known together with other anionic

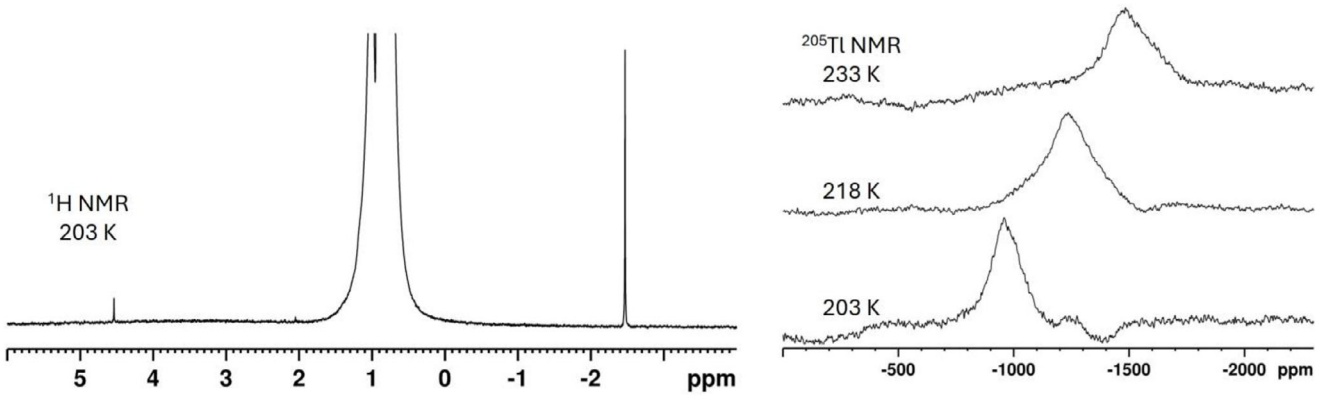

Figure 8. ^{1}H-NMR (left) of the sample $K_8Rb_2Tl_7$ in liquid ammonia at 203 K and ^{205}Tl-NMR (right) at 203 K, 218 K, and 233 K.

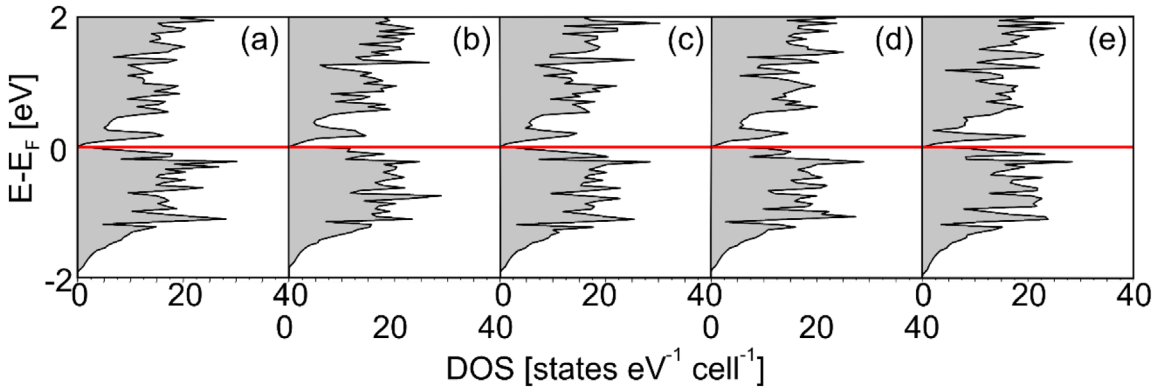

Figure 9. Density of states of K_7Tl_5 a), K_6CsTl_5 b), K_6RbTl_5 c), $K_4Rb_2Tl_5$ d), and Rb_7Tl_5 e) in the area between −2 and 2 eV.

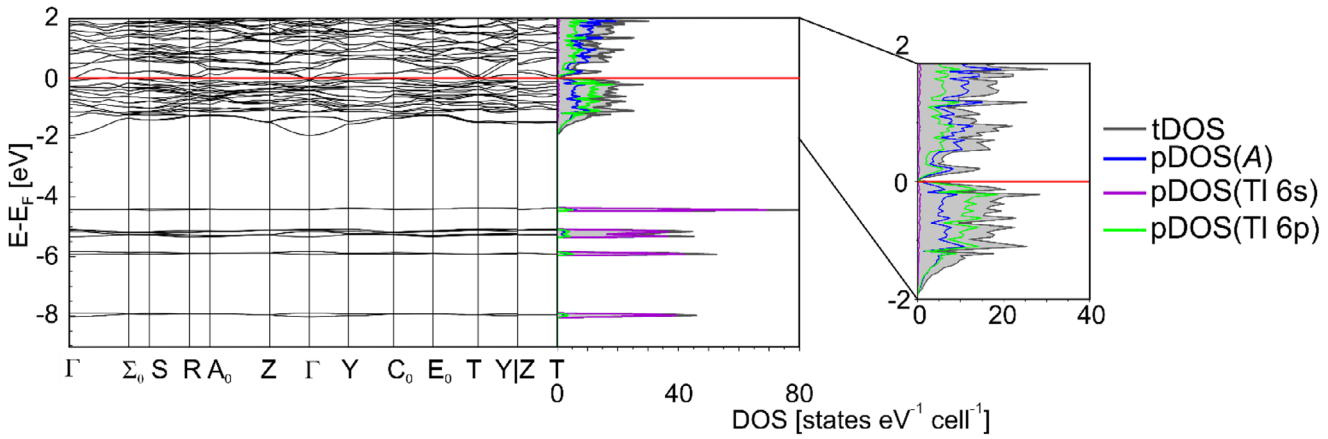

Figure 10. Band structure and DOS (black) with the pDOS of the alkali metals (blue), thallium 6 s (purple), and 6p orbitals (green) of K_6RbTl_5 in the area of −9 to 2 eV and −2 to 2 eV.

moieties. In $K_{7-x}A_xTl_5$, the clusters are arranged in an ABAB stacking sequence, which corresponds to a hcp. Different temperature programs indicated metastability of this phase, which was also proven by DSC and temperature-dependent PXRD measurements. Density functional theory calculations have been performed for the hypothetical compounds without mixed-occupied alkali metal positions, which showed a pseudo band gap at E_F and suggest classical semi-metallic character of the phase. Solvation tests in liquid ammonia showed an oxidation of the alkali metal thallide to elemental thallium after two months. First ^{205}Tl-NMR spectroscopy in liquid ammonia solution allowed for the detection of the first NMR signal emerging from a trielide Zintl phase. Future investigations on the dissolution of salt-like Zintl phases of group 13 in liquid ammonia will show similarities and/or discrepancies compared to the well-established solution chemistry of group 14 and 15 Zintl phases.

4. Experimental Section

Preparation: Potassium (Sigma–Aldrich, purity 98%, under mineral oil) was segregated for purification. Rubidium and cesium were obtained by the reduction of RbCl or CsCl with elemental calcium[58] and were afterward purified through distillation twice. Thallium drops (ABCR, purity 99.999%) were used without further purification and stored under an inert gas atmosphere.

The high-temperature solid-state syntheses were carried out in sealed tantalum ampoules (WHS Sondermetalle GmbH & Co. KG, Germany) using the elements under an argon atmosphere. The sealed ampoules were placed in quartz glass tubes (QSIL GmbH, Ilmenau, Germany) and sealed under an argon atmosphere. Different temperature programs (TP) were used.

TP1 (based on $K_{10}Tl_7$)[33]: heating to 773.15 K, holding for 48 hours, quenching in water, annealing at 393.15 K for 2 weeks, subsequently at 373.15 K for one week, and then cooling to room temperature with 5 K per hour.

TP2: heating to 773.15 K, holding for 48 hours, and quenching in water.

TP3: heating to 773.15 K, holding for 24 hours, cooling to 573.15 K, holding again for 10 hours, and quenching in water.

Compositions of prepared samples and the temperature programs used: K_9RbTl_7 (TP1), $K_8Rb_2Tl_7$ (TP1), K_6RbTl_5 (TP1), K_6RbTl_5 (TP2), K_6CsTl_5 (TP1), K_6CsTl_5 (TP2), $K_{6.8}Rb_{0.2}Tl_5$ (TP2), $K_{6.8}Cs_{0.2}Tl_5$ (TP2), $K_4Rb_3Tl_5$ (TP3), $K_4Cs_3Tl_5$ (TP3), $K_2Rb_5Tl_5$ (TP1), $K_2Cs_5Tl_5$ (TP1), K_7Tl_5 (TP1), Rb_7Tl_5 (TP1), and Cs_7Tl_5 (TP1).

Single-crystal x-ray diffraction (SCXRD): A small number of crystals were transferred into dried mineral oil. From these, a suitable crystal was selected and mounted on a Rigaku SuperNova diffractometer (X-ray: Mo/Ag microfocus, AtlasS2 detector) or a Rigaku XtaLAB Synergy R DW system diffractometer (X-ray: Cu/Mo rotating

anode, HyPix-Arc 150 detector) (Rigaku Polska Sp. z. o. o. UI, Wroclaw, Poland) using *MiTeGen* loops. All data were collected at 123 K.

CrysAlisPro (version 171.43.105a) was used for data collection and data reduction.[59] *ShelXT* was used for the structure solution, and subsequent data refinement was carried out with *ShelXL*.[60,61] Olex^2 was used for visualization purposes,[62] and the software *Diamond4* was chosen for representing the crystal structure.[63] All atoms are depicted as ellipsoids with a 50% probability level.

Deposition Numbers 2464818 ($K_{5.58}Cs_{1.43}Tl_5$), 2464819 ($K_{6.03}Cs_{0.97}Tl_5$), 2464820 ($K_{6.33}Rb_{0.67}Tl_5$), and 2464825 ($K_{4.65}Rb_{2.35}Tl_5$) contain the supplementary crystallographic data for this paper. These data are provided free of charge by the joint Cambridge Crystallographic Data Centre and Fachinformationszentrum Karlsruhe http://www.ccdc.cam.ac.uk/structures.

Powder x-ray diffraction (PXRD): Due to the sensitivity to air and moisture of all samples, they were prepared in sealed capillaries (0.3 mm, WJM-Glas–Müller GmbH, Berlin, Germany). The data collection was carried out on an STOE Stadi P diffractometer (STOE, Darmstadt, Germany) (monochromatic Mo Kα1 radiation, $\lambda = 0.70926$ Å) equipped with a Dectris Mythen 1 K detector. For visualization and indexation, *WinXPOW* and *Jana2006* software were used.[64,65]

DFT calculations: The program FPLO21 was used for DFT calculations.[53–56] It is based on the full-potential nonorthogonal local orbital minimum-basis within the generalized gradient approximation (GGA) for the full relativistic mode. A full relativistic approach is necessary due to the high spin orbit coupling of heavy elements (Cs, Rb, Tl) in these compounds. The exchange correlation was assumed in the form proposed by Perdew, Burke, and Ernzerhof (PBE).[66] For the band structure calculation, $6 \times 6 \times 6$ k-points were used. To visualize the band structure, the program *xfbp* was used, and the DOS was plotted with *Origin2022* (version 9.9.0.225).[67]

SEM/EDS measurements: The crystals for the SEM/EDS measurements were prepared and selected in a glove box under inert gas atmosphere. The measurements were performed on a Zeiss EVO MA15 (Carl Zeiss Microscopy Deutschland GmbH, Oberkochen) using the software *SmartSEM* Version 6.05 with accelerating voltage of 20 kV.[68] For EDS measurements, a Bruker Quantax 200-Z3 Xflash630 (Bruker Corporation, Billerica, USA) was used as X-ray detector with the software *Bruker Esprit 2.1.2*.

DSC measurements: Differential scanning calorimetry (DSC) measurements were performed using a TA Instruments Q200 analyzer. DSC analysis was carried out under a flow of nitrogen (sample purge flow: N_2 40 mL/min). The sample was sealed in a fume hood using a TA Instruments Tzero hermetic aluminium pan, and one heating/cooling cycles were performed from 293.15 K to 773 K at a 5 K/min heating and 1 K/min cooling rate.

Dissolution experiments in liquid ammonia: The experiments were carried out in Schlenk flasks, which were flame-dried three times before adding a small amount of the samples with nominal compositions K_6RbTl_5, K_6CsTl_5, and $K_8Rb_2Tl_7$. After that, dry liquid ammonia was condensed at about 195 K on the products using Schlenk technique. After storing the vessel at 233 K for two months, liquid ammonia was evaporated from the one with K_6CsTl_5. The residue was removed from the Schlenk in the glove box, and a small amount was put in a glass capillary (0.3 mm) for powder diffraction investigations.

NMR measurements: $K_{6.33}Rb_{0.67}Tl_5$ (10 mg, 0.0052 mmol) was put into a baked out heavy-wall precision NMR sample tube (Pyrex) under argon atmosphere. Subsequently, anhydrous ammonia was condensed on the solid-state material and the NMR tube was flame sealed. The sample was stored at 233 K prior to NMR examination, and spectra were recorded on a Bruker AVANCE III HD 400 MHz spectrometer.

Supporting Information

The authors have cited additional references within the Supporting Information.[30–32]

Acknowledgments

The authors thank Prof. Dr. N. Korber and Prof. Dr. A. Pfitzner for providing lab equipment, Dr. Marc Schlosser for conducting the SEM/EDS and HT-PXRD measurements. Additionally, the authors are grateful for funding by the Deutsche Forschungsgemeinschaft (DFG, German Research Foundation) 468336522 and support by the Hans Böckler Foundation (Maria–Weber–Grant for S.G.). T.K. and J.M. would like to thank the project Quantum materials for applications in sustainable technologies (QM4ST), funded as project No. CZ.02.01.01/00/22_008/0004572 by P JAK, call Excellent Research.

Open access funding enabled and organized by Projekt DEAL.

Conflict of Interest

The authors declare no conflict of interest.

Data Availability Statement

The data that support the findings of this study are available in the supplementary material of this article.

Keywords: alkali metals · DFT · DSC · NMR spectroscopy · thallium · X-ray diffraction · Zintl phases

[1] K. Wade, *Nucl. Chem. Lett.* **1972**, *8*, 559.
[2] K. Wade, *Adv. Inorg. Radiochem.* **1976**, *18*, 1.
[3] D. M. P Mingos, *Acc. Chem. Res.* **1984**. *17*, 311.
[4] W. Klemm, *Proc. Chem. Soc. London* **1958**, 329, https://doi.org/10.1039/PS9580000329
[5] R. Nesper, *Anorg. Allg. Chem.* **2014**, *640*, 2639.
[6] H. Schäfer, B. Eisenmann, W. Müller, *Angew. Chem. Int. Ed.* **1973**, *12*, 694.
[7] S. Gärtner, N. Korber, *Zintl Ions Principles and Recent Developments*, (Ed.: T.F. Fässler), **2011**, Springer-Verlag: Berlin Heidelberg, Germany. pp. 25–56.
[8] S. M. Kauzlarich, *Chemistry, Structure and Bonding of Zintl Phases and Ions*, **1996**, VCH, Weinheim.
[9] S. Dehnen, S. M. Kauzlarich, L. Xu, S.-Q. Xia, *Inorg. Chem.* **2024**, *63*, 20051.
[10] T. F. Fässler, *Z. Anorg. Allg. Chem.* **2023**, *650*, e202300227.
[11] E. Zintl, H. Kaiser, *Z. Anorg. Allg. Chem.* **1933**, *211*, 113.
[12] E. Zintl, J. Goubeau, W. Dullenkopf, *Z. Phys. Chem. A* **1931**, *154*, 1.

[13] E. Busmann, *Z. Anorg. Allg. Chem.* **1961**, *313*, 90.
[14] H. G. von Schnering, J. Llanos, J.-H. Chang, K. Peters, E.-M. Peters, R. Nesper, *Z. Kristallogr. NCS* **2005**, *220*, 324.
[15] H. G. von Schnering, M. Schwarz, J.-H. Chang, K. Peters, E.-M. Peters, R. Nesper, *Z. Kristallogr. NCS* **2005**, *220*, 525.
[16] C. Lorenz, S. Gärtner, N. Korber, *Crystals* **2018**, *8*, 276.
[17] S. Gärtner, N. Korber, *Comprehensive Inorganic Chemistry* II(Second ed.) (Eds.: J. Reedijk, K. Poeppelmeier), **2013**, Elsevier, Amsterdam, pp. 251–267.
[18] T. F. Fässler, *Zintl Ions: Principles and Recent Developments* (Ed.: T. F. Fässler), **2011**, pp. 91–131.
[19] C. Hoch, M. Wendorff, C. Röhr, *J. Alloys Compd.* **2003**, *361*, 206.
[20] V. Queneau, E. Todorov, S. C. Sevov, *J. Am. Chem. Soc.* **1998**, *120*, 3263.
[21] S. Gärtner, M. Witzmann, C. Lorenz-Fuchs, R. M. Gschwind, N. Korber, *Inorg. Chem.* **2024**, *63*, 20240.
[22] M. Somer, W. Carrillo-Cabrera, E.-M. Peters, K. Peters, M. Kaupp, H. G. von Schnering, *Z. Anorg. Allg. Chem.* **1999**, *625*, 37.
[23] J. M. Goicoechea, S. C. Sevov, *J. Am. Chem. Soc.* **2004**. *126*, 6860.
[24] S. Joseph, C. Suchentrunk, N. Korber, *Z. Naturforsch. B* **2010**, *65*, 1059.
[25] J. D. Corbett, P. A. Edwards, *Chem. Commun.* **1975**, *24*, 984.
[26] P. A. Edwards,. J. D. Corbett, *Inorg. Chem.* **1977**, *16*, 903.
[27] C. Suchentrunk, N. Korber, *New J. Chem.* **2006**, *30*, 1737.
[28] M. Ruck, F. Steden, *Z. Anorg. Allg. Chem.* **2007**, *633*, 1556.
[29] E. Ahmed, D. Köhler, M. Ruck, *Z. Anorg. Allg. Chem.* **2009**, *635*, 297.
[30] Z. C. Dong, J. D. Corbett, *Inorg. Chem.* **1996**, *35*, 3107.
[31] D. P. Huang, J. D. Corbett, *Inorg. Chem.* **1999**, *38*, 316.
[32] Z. C. Dong, J. D. Corbett, *J. Am. Chem. Soc.* **1994**, *116*, 3429.
[33] S. Kaskel, J. D. Corbett, *Inorg. Chem.* **2000**, *39*, 778.
[34] U. Häussermann, C. Svensson, S. Lidin, *J. Am. Chem. Soc.* **1998**, *120*, 3867.
[35] S. C. Sevov, J. D. Corbett, *Inorg. Chem.* **1991**, *30*, 4875.
[36] W. Blase, G. Cordier, V. Müller, U. Häußermann, R. Nesper, M. Somer, *Z. Naturforsch. B* **1993**, *48*, 754.
[37] R. W. Henning, J. D. Corbett, *Inorg. Chem.* **1997**, *36*, 6045.
[38] M. Falk, A. El Addad, C. Röhr, *25th annual conference of the German Crystallographic Society*, **2017**, De Gruyter: Karlsruhe, Germany, p. 112.
[39] Z.-C. Dong, J. D. Corbett, *J. Cluster Sci.* **1995**, *6*, 187.
[40] S. M. Tiefenthaler, M. Schlosser, F. Pielnhofer, I. G. Shenderovich, A. Pfitzner, S. Gärtner, *Z. Anorg. Allg. Chem.* **2020**, *646*, 82.
[41] E. Zintl, W. Dullenkopf, *Z. Phys. Chem. B* **1932**, *16*, 195.
[42] V. F. Schwinghammer, S. A. Khan, S. M. Tiefenthaler, T. Kovářík, J. Minár, S. Gärtner, *Inorg. Chem.* **2025**, *64*, 6879.
[43] V. F. Schwinghammer, S. Gärtner, *Inorg. Chem.* **2024**, *63*, 20078.
[44] M. Janesch, V. F. Schwinghammer, I. G. Shenderovich, S. Gärtner, *Z. Anorg. Allg. Chem.* **2023**, *649*, e202300112.
[45] V. F. Schwinghammer, M. Janesch, N. Korber, S. Gärtner, *Z. Anorg. Allg. Chem.* **2022**, *648*, e202200332.
[46] Z. C. Dong, J. D. Corbett, *J. Am. Chem. Soc.* **1993**, *115*, 11299.
[47] Z. C. Dong, J. D. Corbett, *Inorg. Chem.* **1996**, *35*, 2301.
[48] C. A. Kraus, *J. Am. Chem. Soc.* **1907**, *29*, 1557.
[49] V. Streitferdt, S. M. Tiefenthaler, I. G. Shenderovich, S. Gärtner, N. Korber, R. M. Gschwind, *Eur. J. Inorg. Chem.* **2021**, *2021*, 3684.
[50] S. M. Tiefenthaler, V. Streitferdt, J. Baumann, S. Gärtner, R. M. Gschwind, N. Korber, *Z. Anorg. Allg. Chem.* **2020**, *646*, 1595.
[51] C. Lorenz, S. Gärtner, N. Korber, *Z. Anorg. Allg. Chem.* **2017**, *643*, 141.
[52] G. W. Watt, G. D. Barnett, L. Vaska, *Ind. Eng. Chem.* **1954**, *46*, 1022.
[53] H. Eschrig, K. Koepernik, I. Chaplygin, *J. Solid State Chem.* **2003**, *176*, 482.
[54] K. Koepernik, H. Eschrig, *Phys. Rev. B* **1999**, *59*, 1743.
[55] K. Lejaeghere, G. Bihlmayer, T. Björkman, T. Blaha, S. Blügel, V. Blum, D. Caliste, I. E. Castelli, S. J. Clark, A. Dal Corso, S. de Gironcoli, T. Deutsch, J. K. Dewhurst, I. Di Marco, C. Draxl, M. Dułak, O. Eriksson, J.-A. Flores-Livas, K. F. Garrity, L. Genovese, P. Giannozzi, M. Giantomassi, S. Goedecker, X. Gonze, O. Grånäs, E. K. U. Gross, A. Gulans, F. Gygi, D. R. Hamann, P. J. Hasnip, N. A. W. Holzwarth, D. Iuşan, D. B. Jochym, F. Jollet, D. Jones, G. Kresse, K. Koepernik, E. Küçükbenli, Y. O. Kvashnin, I. L. M. Locht, S. Lubeck, M. Marsman, N. Marzari, U. Nitzsche, L. Nordström, T. Ozaki, L. Paulatto, C. J. Pickard, W. Poelmans, M. I. J. Probert, K. Refson, M. Richter, G.-M. Rignanese, S. Saha, M. Scheffler, M. Schlipf, K. Schwarz, S. Sharma, F. Tavazza, P. Thunström, A. Tkatchenko, M. Torrent, D. Vanderbilt, M. J. van Setten, V. Van Speybroeck, J. M. Wills, J. R. Yates, G.-X. Zhang, S. Cottenier, *Science* **2016**, *351*, 7.
[56] I. Opahle, K. Koepernik, H. Eschrig, *Phys. Rev. B* **1999**, *60*, 14035.
[57] K. Finzel, U. Schwarz, *Inorg. Chem.* **2024**, *63*, 20217.
[58] L. Hackspill, *Cr. Hebd. Acad. Sci.* **1905**, *141*, 106.
[59] M. W. Schneider, I. M. Oppel, A. Griffin, M. Masalerz, CrysAlisPRO, Oxford Diffraction /Agilent Technologies UK Ltd: Yarnton, UK, **2020**.
[60] G. M. Sheldrick, *Acta Crystallogr. A* **2015**, *71*, 3.
[61] G. M. Sheldrick, *Acta Crystallogr. C* **2015**, *71*, 3.
[62] O. V. Dolomanov, L. J. Bourhis, R. J. Gildea, J. A. K. Howard, H. Puschmann, *J. Appl. Crystallogr.* **2009**, *42*, 339.
[63] K. Brandenburg, Diamond, Crystal Impact GbR, Bonn, **2021**.
[64] A. Toombs, S. WinXPOW, C. GmbH, Darmstadt, **2016**.
[65] V. Petrícek, M. Dusek, L. Palatinus, *Z. Krist.-Cryst. Mater.* **2014**, *229*, 345.
[66] J. P. Perdew, K. Burke, M. Ernzerhof, *Phys. Rev. Lett.* **1996**, *77*, 3865.
[67] Origin(Pro), OriginLab Corporation, Northampton, MA, USA, **2022**.
[68] SmartSEM, Carl Zeiss Microscopy Deutschland GmbH, Oberkochen.

Manuscript received: September 14, 2025
Revised manuscript received: October 8, 2025
Version of record online: ■■, ■■